STP 1203

Fractography of Modern Engineering Materials: Composites and Metals, Second Volume

John E. Masters and Leslie N. Gilbertson, editors

ASTM Publication Code Number (PCN)
04-012030-30

ASTM
1916 Race Street
Philadelphia, PA 19103

ISSN: 1071-5827
ISBN: 0-8031-1866-X
ASTM Publication Code Number (PCN): 04-012030-30

Photocopy Rights

Peer Review Policy

Each paper published in this volume was evaluated by three peer reviewers. The authors addressed all of the reviewers' comments to the satisfaction of both the technical editor(s) and the ASTM Committee on Publications.

The quality of the papers in this publication reflects not only the obvious efforts of the authors and the technical editor(s), but also the work of these peer reviewers. The ASTM Committee on Publications acknowledges with appreciation their dedication and contribution to time and effort on behalf of ASTM.

Printed in Fredericksburg, Virginia
December 1993

Foreword

The Second Symposium on Fractography of Modern Engineering Materials II was held May 6, 1992 in Pittsburgh, Pennsylvania. The symposium was held in conjunction with the May 4–7, 1992 standards development meetings of ASTM Committees D-30 and E-24, the symposium sponsors. John E. Masters and Leslie N. Gilbertson served as symposium co-chairmen and as editors of this publication.

Contents

Overview

This book contains the manuscripts of eleven papers that were presented at the Second Symposium on Fractography of Modern Engineering Materials held in May 1992. The numerous advances in materials science in the six year period following the First Symposium dictated this second meeting. Not only had new materials been developed in the intervening years, but understanding of older materials had also progressed. Similarly, advances in the technology and the techniques of fractography had occurred. The objective of the symposium was to extend the colloquy on fractography to include these many advances.

The papers may be divided into three sections: Unique Fractographic Techniques; Metallic Materials; Polymeric and Composite Materials. The section titles reflect the diversity of materials discussed in the meeting. The range of materials included cross-linked polyethylene, AISI 52100 steel, 2024 aluminum, and a variety of organic and metal matrix fibrous composites. The case studies presented also covered a wide range. They included failure investigations of an antenna used in deep space exploration and chemical storage tanks. Advances in the techniques of fractography were also reflected in a number of presentations; quantitative techniques and expert systems were also subjects of presentations.

A short precis of each paper is included here to assist the readers in identifying works of particular interest.

Unique Fractographic Techniques

As in other technologies, the computerization of the workplace has had a profound effect on fractography and failure analysis.

Using digital image analyses of fracture profiles, Gokhale et al., for example, were able to estimate fracture surface topographic parameters such as roughness, and anisotropy via quantitative fractographic techniques. The authors indicate that these parameters can, in turn, be related to material toughness to establish relationships of structure to properties.

In a related paper, Drury and Gokhale addressed issues of implementing profilometric studies. They specifically focused on the statistical aspects of measuring surface roughness, fractal dimension, and other geometric descriptors. The results of this work led to the proposal of a profilometry sampling criteria which could serve as guidelines for future quantitative fractographic studies.

The final paper in this section discusses the development of an expert system that guides the user in establishing potential failure modes in fiberglass-reinforced polymeric materials used in the automotive industry. The authors, Saliba and Saliba, also developed a computerized atlas which displays photomicrographs for user-specified materials, environmental conditions, and failure modes.

Metallic Materials

Fatigue crack growth was a theme common to all three papers presented in this section on the failure analysis of metallic materials.

Ranganathan et al. discusses a quantitative analysis of fatigue fracture surfaces they developed by studying 2024 T351 aluminum specimens subjected to constant amplitude and variable amplitude loading. The effects of applied stress intensity factor, K, and the stress ratio, R, can be quantified using this technique.

The paper by DiGiorgio and Hsieh demonstrates a holistic approach to failure analysis of complex systems. This approach looks at the overall system in which the component failed to find the full real reasons for failure. In the failure of roller bearings on a radio telescope system, the authors established fatigue as the initiating cause of fracture of the roller. Stress raisers at a center through-bore hole accentuated the applied load. The authors were able to relate modifications in the radio telescope system to increased loads that pushed inherent flaws beyond the critical level for the roller bearing material.

Sundar et al. conducted a fractographic study of short crack growth in notched 2014 T5511 aluminum alloy. They studied the fracture surfaces using both optical microscopy and transmission electron microscopy of replicas. Their work showed that short notch root fatigue cracks will open at considerably lower stress levels than the stress associated with the onset of crack closure.

Polymeric and Composite Materials

The widespread application of polymeric and composite materials in industry was reflected in the number of papers that discussed these materials.

Wachob et al. reviewed their failure analyses of cross linked polyethylene (XLPE) storage tanks used for long-term storage of chemically active solutions. The physical, mechanical, and chemical evidence they gathered indicated that XLPE can be severely oxidized and degraded when concentrated industrial bleach or oxidizing acids decompose or react with it.

The tensile and tension-tension fatigue fractures of continuous γ-Al_2O_3 fiber reinforced aluminum-based metal matrix composites were the subject of the investigation reported by Komai et al. They examined a number of 0°, 90°, 0°/90°, and $\pm 45°$ laminates tested at both room temperature and at 573°K and identified the controlling failure mechanisms.

Macheret et al. studied damage development in aramid fiber-reinforced aluminum laminates made of thin aluminum sheets alternated with plies of epoxy prepreg containing unidirectional aramid fibers. They presented fatigue crack growth data on surface notch and open hole initiated fatigue cracks. Their failure analysis revealed that the surface initiated cracks propagated only in the outer aluminum layer; the fibers remained intact. Cracks initiated at the open hole, on the other hand, propagated through the laminate thickness in all aluminum layers. This, they noted, could lead to complete fiber failure depending on the laminate residual stress state.

Pinell et al. investigated the axial compression response of two different quasi-isotropic graphite epoxy layups, $[0/+45/90/-45]$s and $[0°/\pm 60°]$s, using both a miniature sandwich specimen and an all-laminate specimen. They were able to identify the initial damage mechanisms and define the sequence of failure events through a combination of fractographic and mechanical analyses.

The final paper reviews the results of an investigation of the fracture surfaces of Cracked Lap Shear Coupons made of graphite epoxy and graphite polyetheretherketone (PEEK) composite material. In this work, Fortson and Armanios applied quantitative fractographic techniques to track the area fractions of four fracture morphologies as a function of position on the fracture surface. Their efforts support the validity of the specimen configuration as a test specimen.

In closing, it is hoped that the papers presented in this volume will aid investigators in conducting failure investigations. It is also hoped that additional symposia will be held as this body of knowledge continues to be developed.

The editors would like to gratefully acknowledge the many contributions provided to this volume by the authors, the reviewers, and ASTM staff, Monica Siperko and Rita Hippensteel.

John E. Masters
Lockheed Engineering and Science
Hampton, Virginia
Symposium Co-chairman and Co-editor

Leslie N. Gilbertson
Zimmer, Inc.
Warsaw, Indiana
Symposium Co-chairman and Co-editor

A. M. Gokhale,[1] *W. J. Drury,*[1] *and S. Mishra*[1]

Recent Developments in Quantitative Fractography

REFERENCE: Gokhale, A. M., Drury, W. J., and Mishra, S., **"Recent Developments in Quantitative Fractography,"** *Fractography of Modern Engineering Materials: Composites and Metals, Second Volume, ASTM STP 1203,* John E. Masters and Leslie N. Gilbertson, Eds., American Society for Testing and Materials, Philadelphia, 1993, pp. 3–22.

ABSTRACT: Quantitative characterization of fracture surface topography is an important aspect of quantitative fractography. This contribution is concerned with the profilometric methods for the estimation of the important descriptors of the fracture surface topography. The parameters such as fracture surface roughness, tortuosity, fraction overlap, etc. are defined, and the profilometric measurements that enable the estimation of such parameters are described. Recent experimental data on the surface roughness and fractal dimension pertaining to creep and impact fracture surfaces are presented to demonstrate the utility of the topographic parameters.

KEYWORDS: quantitative fractography, topography, creep, impact fracture

The geometry and topography of the fracture surface are often dictated by the microstructural features and the failure mechanisms that govern the fracture. Thus, the study of the fracture surfaces, that is, fractography, provides an important input for understanding the fracture processes. With the development of modern scanning electron microscopy (SEM), fractography has become an important tool for failure analysis as well. The qualitative SEM fractographic observations have provided crucial input for our present understanding of the fracture processes. "Quantitative" fractography may yield similar dividends in the future materials research. The quantitative fractography is concerned with the quantitative characterization of the geometric attributes of the fracture surface topography (for example, roughness, tortuosity, etc.) and the microstructural features that are present on the fracture surface (number density, average size, etc.). It is the purpose of this paper to present the recent developments in the quantitative fractography that are concerned with the characterization of the fracture surface topography. The earlier attempts to quantify fracture surface topography involved the individual features such as striation spacings. Such analyses are said to employ "local measurements" [*1,2*]. The present paper is, however, concerned with the recent results which involve the measurements of "global" geometric attributes of fracture surface (for example, surface roughness). The global properties can be estimated without any assumptions concerning the geometry in an unbiased manner, and hence, may yield true correlations with the deformation and fracture mechanisms.

The quantitative descriptors of fracture surface topography are defined in the first section of the paper. These parameters are "global" in nature. The experimental techniques of fracture profilometry are described in the second section. The third section of the paper deals with the relationships between the profilometric data and the descriptors of fracture surface geometry which enable assumption-free and unbiased estimates of these parameters. Some recent experimental data are

[1]School of Materials Engineering, Georgia Institute of Technology, Atlanta, GA 30332.

discussed in the last two sections to demonstrate the applications of the quantitative fractographic measurements.

Descriptors of Fracture Surface Topography

The co-ordinates of the set of points on the fracture surface contain complete information on the surface topography. However, in practice, it is of interest to describe the surface characteristics in terms of a few quantitative parameters which can be defined uniquely, and can be measured in an assumption-free and unambiguous manner using simple metallographic procedures. It is important that these quantitative parameters are physically meaningful as well, so that they can be correlated to the material properties and microstructure. The most meaningful attributes of the fracture surface are its roughness, tortuosity, extent of re-entrant regions or overlaps, and anisotropy. The work of fracture of brittle solids is directly related to fracture surface roughness (higher roughness implies higher surface area). The fracture surface tortuosity is related to the extent of crack deflection [*3,4*] and it correlates with the absorbed energy in the impact test specimens. The extent of re-entrant regions correlate well with amount of creep damage [*5,6*].

Fracture Surface Roughness

Consider a fracture surface enclosed in a reference volume as shown in Fig. 1. Let S_o be the true area of the fracture surface. Let Z axis be normal to the average topographic plane of the fracture surface, and let A be the apparent projected area of the fracture surface on this average topographic plane (flat face of the cylinder in Fig. 1). The surface roughness is quantified by the surface roughness parameter R_s defined as follows [*7,8*]

$$R_s = \frac{S_o}{A} \tag{1}$$

For a flat surface R_s is equal to one. In general, the rougher the surface, the higher is the value of R_s. Theoretically, R_s can have any value in the range of one to infinity. Measurement of R_s essentially involves the measurement of fracture surface area, and hence it can be utilized to estimate the fractal dimension [*9*] of the surface. Recently, Baggerly [*10,11*] has reported a strong correlation between R_s and the stress intensity amplitude ΔK during fatigue crack growth in ductile cast iron. The image of a fracture surface observed by SEM is essentially the projected image. For example, the projected area "A" would be observed in the SEM image of the fracture surface shown in Fig. 1. Thus, some quantitative measurements performed on SEM fractographs require the reference area correction. For example, let N_A be the number of inclusions per unit area of SEM fractograph. The "true" value of the number of inclusions per unit area of fracture surface N_s is related to N_A as follows.

$$N_s = \frac{N_A}{R_s} \tag{2}$$

According to Underwood [*12,13*] a very significant error (bias) may result if the SEM fractographic measurements of the number density are not normalized by the roughness parameter R_s. Thus, R_s is an essential auxiliary input required for valid SEM quantitative fractographic measurements.

Fracture Surface Tortuosity

In principle, the fracture surface area can be estimated by laying a square areal grid on the fracture surface, and counting the number of squares: the area of each square multiplied by the number of squares gives an estimate of the fracture surface area. It is obvious that the surface area

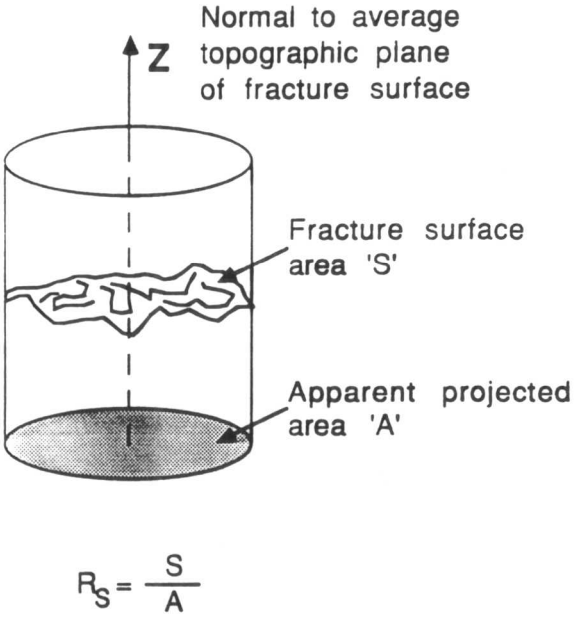

FIG. 1—*Concept of fracture surface roughness parameter.*

estimated in this manner will vary with the size of the unit square; the finer grid is expected to yield a higher value of the surface area. The surface roughness parameter R_s is directly proportional to the surface area of the fracture surface, and hence, R_s also depends on the size of the unit square or the resolution of the measuring unit. However, as the size of the unit square approaches infinity, R_s approaches one. Further, as the size of the unit square approaches zero, R_s approaches a saturation value R_s^o. Figure 2 shows variation of R_s with the area of the unit square η^2 schematically. The corresponding experimental data for the fracture surface of a low alloy steel are shown in Fig. 3. Inspection of these figures indicates that there is a range of length scales where R_s increases monotonically with the decrease in the size of the measuring unit η^2; this variation is linear on the

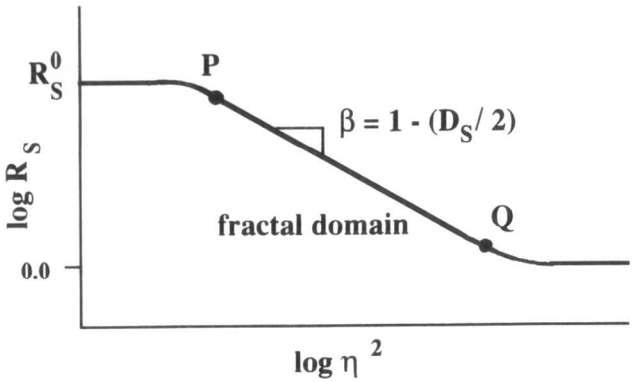

FIG. 2—*Schematic diagram showing variation of R_s with area of unit size, η^2.*

$$dS(\theta,\phi) = S_o\, a(\theta,\phi) \sin\theta d\theta \cdot d\phi/2\pi \tag{6}$$

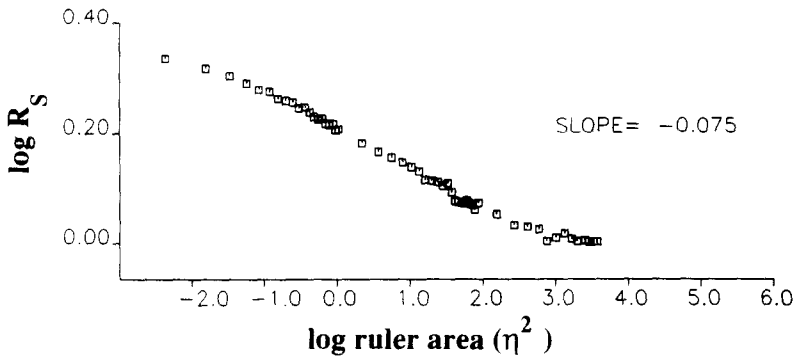

FIG. 3—*Experimental data showing R_s versus η^2 for a fracture surface of AISI 4340 low alloy steel.*

log-log scale (region pq in Figs. 1 and 2), and it can be represented by the following equation [*14,15*].

$$R_s = b[\eta^2]^{2-D_s/2} \tag{3}$$

Equation 3 is nothing but the fractal characteristics proposed by Mandelbrot [*9*] for the fractal surfaces. The quantity (η^2) is the area of the measuring unit, b is a constant, and the parameter D_s is the fractal dimension of the surface. It may be said that the fracture surfaces exhibit fractal behavior over certain regimes of the length scales. The fractal dimension D_s admits values in the range of 2 to 3. A flat surface has fractal dimension equal to 2, and in such a case R_s does not vary with the area of the measuring unit. D_s is related to the RATE at which R_s changes with the area of the measuring unit η^2.

For a featureless fracture surface (for example, fracture surface of glass) there is no significant change in R_s as (η^2) decreases, because there is no more "information" present on the surface. Such a surface has a fractal dimension close to 2, and it has no significant "tortuosity." As the tortuosity of the fracture surface increases (due to crack deflection, etc.), more and more features are resolved at higher and higher resolution level (that is, smaller and smaller values of (η^2)) at an increasing rate, which effectively increases the rate at which the fracture surface area measure (and hence, R_s) increases with the decrease in (η^2), and results in an increase in the fractal dimension D_s. Thus, as the fracture surface tortuosity increases, the surface fractal dimension D_s also increases in a unique manner. Hence, the fracture surface fractal dimension D_s can be used as a quantitative measure of the surface tortuosity. Note that the parameter D_s can be experimentally measured [*14,16*] a technique based on profilometry is described in a subsequent section.

Fraction of Surface Overlap

The fracture surfaces often contain re-entrant or overlapped regions. Figure 4 shows the overlaps in the fracture profile through the fracture surface of copper generated by creep fracture. The overlapped regions of the fracture surface can not be observed by SEM fractography. The overlaps can be observed in the fracture profiles generated by metallographic sectioning of the fracture surface (see Fig. 4). The extent of re-entrant regions or overlaps in the fracture surface can be quantified by the overlap parameter O_s defined as follows.

$$O_s = \frac{S'}{S_o} \tag{4}$$

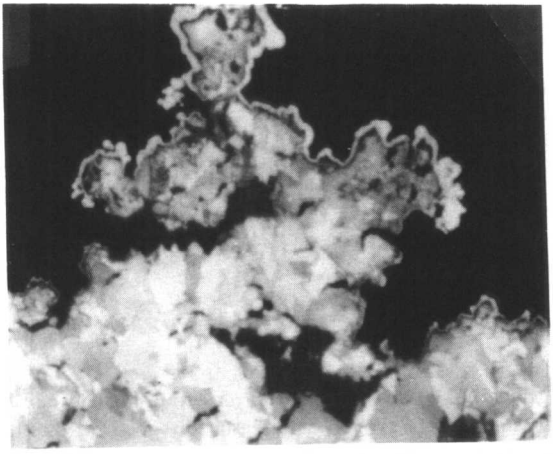

FIG. 4—*Re-entrant regions in a fracture profile obtained from a fracture surface of copper failed in creep.*

S' is the surface area of the re-entrant regions, and S_o is the total surface area of the fracture surface. If O_s is not significantly less than one, then equation 2 needs to be modified to correct for the overlap as follows.

$$N_s = \frac{N_A}{R_s(1 - O_s)} \tag{5}$$

It is possible to experimentally measure the fraction of fracture profile length having re-entrant regions. This data can be utilized to estimate O_s; the details are discussed in a subsequent section.

Fracture Surface Anisotropy

The surface elements on the fracture surface may be randomly oriented, or they may exhibit anisotropy; most of the real fracture surfaces are anisotropic. The extent of fracture surface anisotropy can provide information concerning the fracture processes that generate the anisotropy. Orientation of any given surface element on the fracture surface is given by the orientation of its normal vector. The orientation of the normal vector is specified by the two angles θ and ϕ with respect to the XYZ reference axes, as shown in Fig. 5. The XY plane is the average topographic plane of the fracture surface, and Z-axis the direction normal to the average topographic plane. Let $dS(\theta,\phi)$ be the fracture surface area having the orientation in the range θ to $(\theta + d\theta)$ and ϕ to $(\phi + d\phi)$. The orientation distribution function of the surface elements on the fracture surface $g(\theta,\phi)$ is defined as follows.

$$dS(\theta,\phi) = S_o\, g(\theta,\phi) \sin\theta d\theta \cdot d\phi/2\pi \tag{6}$$

For a randomly oriented fracture surface,

$$g(\theta,\phi) = 1 \tag{7}$$

The orientation distribution function (ODF) quantifies the anisotropy of the surface elements on the fracture surface, and it is similar to probability distribution function. If the ODF is symmetric with

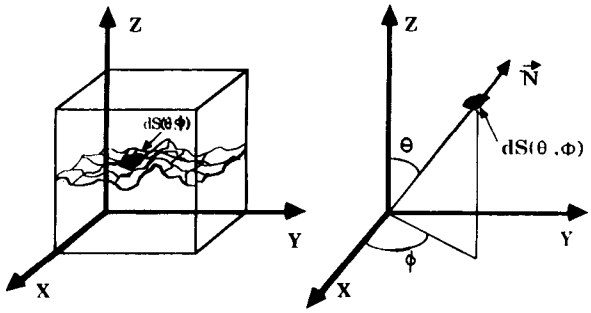

FIG. 5—*Specification of orientation of a surface element on fracture surface.*

respect to the Z axis, then $g(\theta,\phi)$ does not depend on ϕ (all ϕ angles are equally likely), and it depends on θ only. Assumption of symmetry is reasonably good for the fracture surfaces of the materials having isotropic microstructures, and fractured under the stress distribution that has a symmetry axis (for example, fracture surface of annealed copper generated by uniaxial tensile stress). The symmetric ODF can be estimated from the profilometric measurements described in the subsequent section.

Experimental Techniques of Fracture Profilometry

Profilometry is the study of two-dimensional plane sections through fracture surface. Intersection of the fracture surface by a sectioning plane yields an irregular line of complex shape, called fracture profile (see Fig. 6). Depending on the orientation of the sectioning plane, vertical [*17*], horizontal [*18*], or slanted [*19*] profiles can be obtained. Vertical sections are very useful, because the underlying microstructure can be observed simultaneously, and most of the equations that relate the measurements performed on the fracture profiles to the corresponding attributes of the fracture surface require that the measurements be performed on the vertical sections only.

A vertical section is defined as a metallographic section that contains the vertical axis, which is the direction perpendicular to the average topographic plane of the fracture surface (see Fig. 7). The intersection of the fracture surface with the vertical section generates the vertical section fracture profile. In practice, to generate a vertical section fracture profile, the fracture surface is plated with a protective layer such as electroless nickel plating followed by a suitable conventional electroplating such as copper. The specimen is then sectioned along a plane perpendicular to the fracture surface as shown in Fig. 7. The sectioned plane is metallographically prepared using the conventional polishing techniques and the fracture profile is observed in the microscope. A typical fracture profile obtained in this manner is shown in Fig. 6.

The complete information concerning the geometry of the fracture profile is contained in the set of co-ordinates of the points on the fracture profile. These data can be obtained by digitizing the profile via semiautomatic or automatic digital image analysis. Typically, the process involves tracing of the fracture profile using an electronic cursor [*20*]. The image analyzer records the co-ordinates of the points on the fracture profile at preselected fixed intervals; the interval length is called "ruler length." The profile is thus represented by a series of straight line segments as shown in Fig. 8. These raw data can be used to calculate the following via an appropriate software.

(1) The total profile length can be obtained by adding the lengths of all the straight line segments on the fracture profile (see Fig. 8).

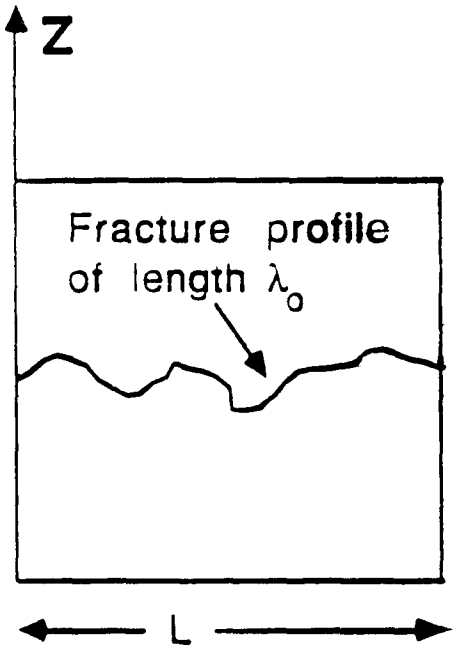

FIG. 6—*Fracture profile generated from fracture surface.*

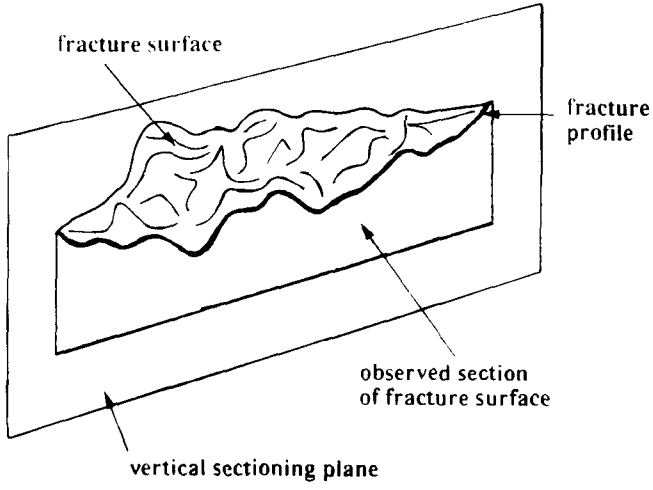

FIG. 7—*Vertical sections through fracture surface.*

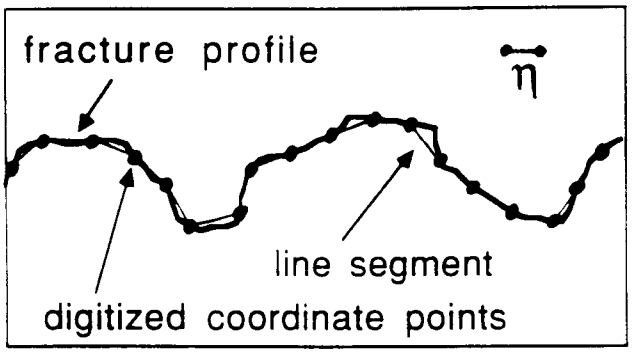

FIG. 8—*Digitized fracture profile and ruler length.*

(2) The vertical axis (that is, the direction normal to the average topographic plane of the fracture surface) can be identified in the vertical section. The angle between this reference direction and each digitized straight line segment on the digitized profile can be calculated, and the angular orientation distribution function of the line elements on the digitized fracture profile can be obtained.

(3) The total digitized profile length often depends on the distance between the consecutive digitized co-ordinate points, that is, the ruler length. It is possible to calculate the total profile length as a function of the ruler length. Such data are useful for the calculation of the fractal dimension of the fracture profile.

The digitized profile data can be used to calculate the important descriptors of the geometry of the fracture profile as given in the following section.

Descriptors of Fracture Profile Topography

The set of co-ordinates of the points on the fracture profile contain complete information concerning the topography of the fracture profile. The following useful parameters can be calculated from such data.

Profile Roughness Parameter

The roughness of the fracture profile is quantified by the profile roughness parameter R_L defined as follows [*7,17*].

$$R_L = \frac{\lambda_o}{L} \tag{8}$$

λ_o is the total profile length and L is the projected length of the profile (see Fig. 6). For a straight line R_L is equal to one. In general, R_L can have any value ranging from one to infinity. The rougher the fracture profile, the higher is the value of R_L. The profile roughness parameter R_L depends on the roughness of the fracture surface AND the orientation of the sectioning plane (that generates the profile) with respect to the fracture surface. Different sectioning planes intersecting same fracture surface can generate the profiles having different values of R_L (see Fig. 9). As the total profile length can be calculated from the digitized co-ordinate data; R_L can be also calculated. Banerji [*21*] has used the profile roughness parameter measurements to study fatigue crack propagation. It is

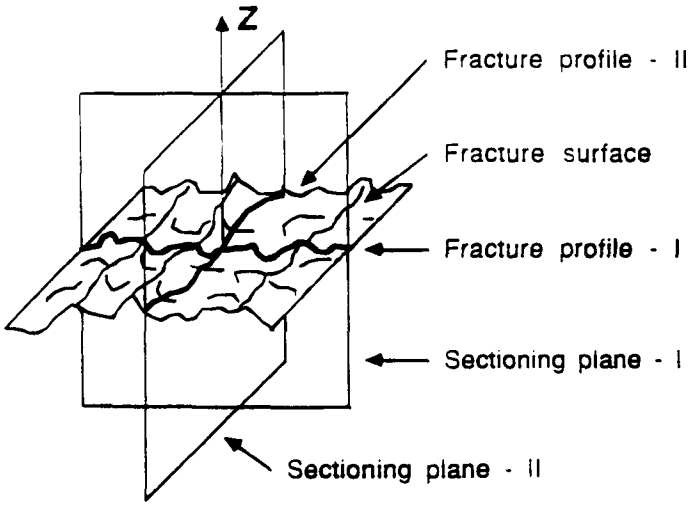

FIG. 9—*Different sectioning planes having different orientations may yield profiles having different R_L values.*

important to emphasize that there is no one to one correlation between R_L and R_s: rougher profile does not necessarily imply a rougher surface. A general procedure to calculate R_s from the measurements performed on the fracture profiles is presented in the next section.

Fractal Dimension of Fracture Profile

The total profile length (and hence, R_L) is calculated by adding the lengths of the straight line segments obtained by joining the consecutive co-ordinate points on the digitized profile (see Fig. 8). Thus, the calculated value of the profile length (and hence, R_L) depends on the distance between the consecutive co-ordinate points η, which is called ruler length. Smaller value of η (that is, closely spaced co-ordinate points) may lead to a larger value of profile length and R_L. The rate at which R_L or profile length changes with η is related to the tortuosity of the fracture profile. However, as η approaches zero, R_L approaches a saturation value (say, R_L^o), and as η becomes very large, R_L approaches one. In the intermediate range of values of η, R_L increases systematically as η decreases. Figure 12 shows the plot of R_L versus η on a log-log scale for a fracture profile of a low alloy steel. In the range of η values where R_L decreases with η, the variation can be represented by the following equation [*9,12,13*].

$$R_L = R_L^* \cdot [\eta]^{1-D_L} \tag{9}$$

R_L^* is a constant, η is the ruler length, and constant D_L is called the fractal dimension of the fracture profile, which is the measure of the tortuosity of the profile. A featureless profile has fractal dimension equal to one. From the digitized co-ordinate data, the total profile length, and hence, R_L, can be calculated for different η values simply by removing the alternate points (which doubles the value of η) and calculating R_L; the procedure can be repeated until only two points are left. The fractal dimension D_L can be then calculated from such data. Banerjee and Underwood [*27*] have shown that the fracture profile fractal dimension is useful for detecting temper embrittlement in low alloy steel.

Profile Angular Orientation Distribution Function

The angular orientation of a line element on the fracture profile is specified by the angle a between the line element and the vertical axis. The orientation angle α can be calculated for each line segment on the digitized fracture profile. The orientation distribution function $f(\alpha)$ is such that $f(\alpha)d\alpha$ is equal to the fraction of profile length having the orientation in the range α to $(\alpha + d\alpha)$. For a randomly oriented fracture profile, $f(\alpha)$ is equal to $1/\pi$, because all the orientations are equally likely. The profile orientation distribution function is required for the estimation of R_s as well as for the estimation of the orientation distribution function of the surface elements on the fracture surface.

Profile Fraction Overlap

Fracture surfaces, and hence the fracture profiles often contain re-entrances or overlaps. For example, the fracture profile of copper specimen failed in creep, shown in Fig. 4 exhibits significant overlaps. The fraction overlap is simply equal to the length of the re-entrant segments of the profile divided by its total length (see Fig. 10).

Relationships Between Profile and Surface Characteristics

The surface roughness parameter R_s can be estimated from the measurements that can be performed on the vertical section fracture profiles by using the following general, assumption-free, and unbiased relationship given by Gokhale and Underwood [*22*]

$$R_s = \overline{\psi \cdot R_L} \tag{10}$$

$$\psi = \int_o^{\pi} \left[\sin\alpha + \left(\frac{\pi}{2} - \alpha \right) \cos\alpha \right] \cdot f(\alpha)\, d\alpha \tag{11}$$

"ψ" is called the profile structure factor. $f(\alpha)$ is the orientation distribution function of the line elements on the fracture profile. In equation 10 the "bar" signifies that the AVERAGE or expected

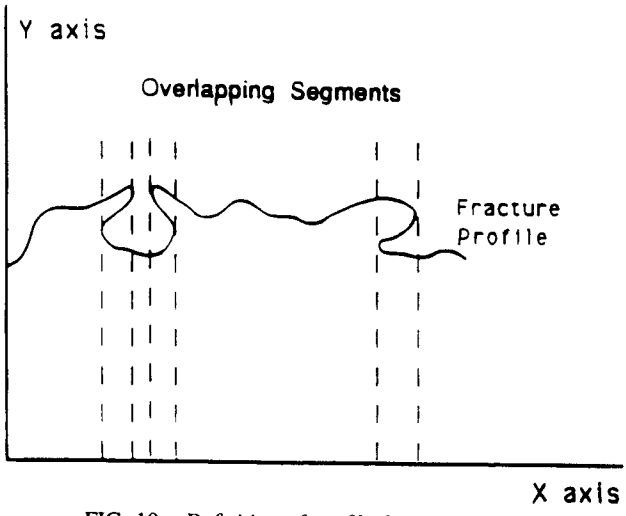

FIG. 10—*Definition of profile fraction overlap.*

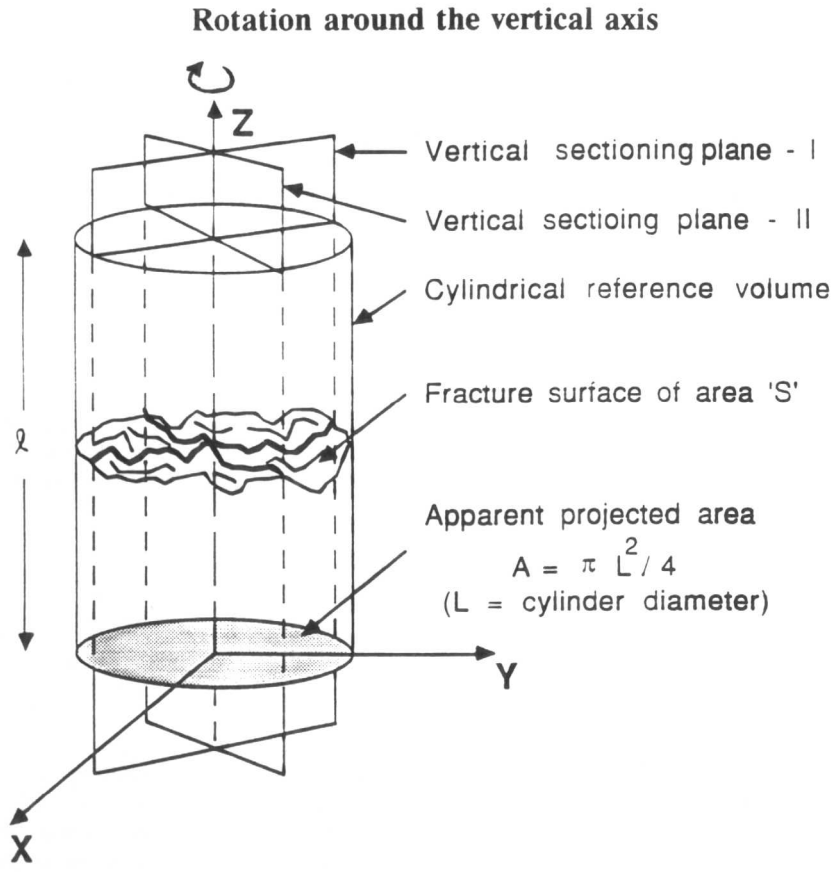

FIG. 11—*Different vertical section orientations involve rotation around the vertical axis.*

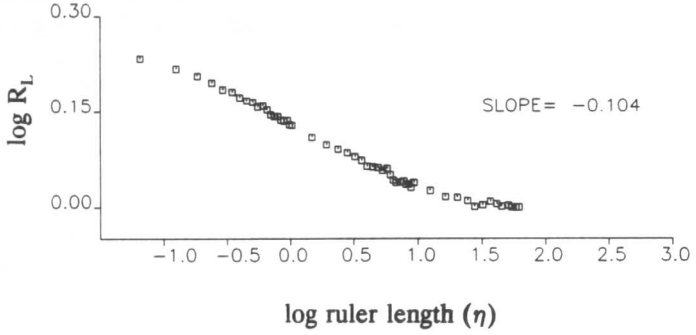

FIG. 12—*Log R_L versus log η for fracture profile of an AISI 4340 low alloy steel.*